Four-wave mixing in Bose-Einstein condensate systems with multiple spin states

J. P. Burke, Jr.,* P. S. Julienne, and C. J. Williams
100 Bureau Drive, Stop 8423, National Institute of Standards and Technology, Gaithersburg, Maryland 20899-8423, USA

Y. B. Band
Department of Chemistry, Ben-Gurion University of the Negev, Beer-Sheva, Israel 84105

M. Trippenbach
Institute of Experimental Physics, Optics Division, Warsaw University, ul. Hoża 69, Warsaw 00-681, Poland
(Received 19 April 2004; published 21 September 2004)

We calculate the four-wave mixing (FWM) in a Bose-Einstein condensate system having multiple spin wave packets that are initially overlapping in physical space, but have nonvanishing relative momentum that causes them to recede from one another. Three receding condensate atom wave packets can result in production of a fourth wave packet by the process of FWM due to atom-atom interactions. We consider cases where the four final wave packets are composed of one, two, three, and four different internal spin components. FWM with one or two-spin state wave packets is much stronger than three- or four-spin state FWM, wherein two of the coherent moving Bose-Einstein condensate wave packets form a spin-polarization grating that rotates the spin projection of the third wave into that of the fourth diffracted wave (as opposed to the one- or two-spin state case where a regular density grating is responsible for the diffraction). Calculations of FWM for ^{87}Rb and ^{23}Na condensate systems are presented.

DOI: 10.1103/PhysRevA.70.033606 PACS number(s): 03.75.Mn, 03.75.Nt, 03.75.Kk

I. INTRODUCTION

The realization of Bose-Einstein condensation (BEC) of dilute alkali-metal gases has created considerable interest in the field of nonlinear atom optics. In a BEC, pairwise atomic collisions whose strength is characterized by the two-body *s*-wave scattering length *a* gives rise to a nonlinear interaction that can produce four-wave mixing (FWM) phenomena. The FWM process allows one to study a variety of phenomena ranging from Bose stimulation [1–3], elastic scattering loss to empty modes [4], entanglement and correlations [5], and squeezing. The first experimental demonstration of FWM of matter waves was reported by Deng *et al.* [1] and involved four BEC wave packets in identical internal spin states. The theory of single spin matter-wave FWM was developed in Refs. [2,3,6,7]. But FWM is also possible for different internal spin states [7], where spin exchange collisions may be involved.

This paper makes predictions about the strength of the signal in multiple spin FWM experiments using a mean field theory with arbitrary internal spin BEC matter wave packets, including both elastic and inelastic loss processes. FWM can occur in BEC systems containing one, two, three, or four different internal spin components. With one- or two-spin states, the process of FWM is analogous to Bragg diffraction of matter waves off a density grating formed by two of the moving BEC wave packets, from which the third wave packet can scatter to produce a fourth wave. We show that the three- or four-spin state case is phenomenologically different from the one- or two-spin state case. In particular, the nonlinear coupling strength of the former depends on differences of scattering lengths, greatly reducing the fourth wave generated by FWM. In this latter case the grating is no longer a density grating but a spin-density grating, i.e., a spin-polarization grating, and the diffraction process rotates the spin projection of the third wave packet into that of a fourth diffracted wave packet. This is in analogy with the situation in nonlinear optics wherein FWM of light waves can occur in nonisotropic media thereby producing a fourth wave by the scattering of one of the input waves from a polarization grating created by the two other input waves, rather than a refractive-index grating created by the two other input waves.

This paper is organized as follows. Section II provides a general description of the process of FWM of multispin Bose-Einstein condensates including the Bragg output coupling technique for generating high momentum wave packets. We review general multispin wave packet coupled equations of motion within the slowly varying envelope approximation (SVEA) and formulate phase matching conditions for multicomponent spin systems. Section III describes calculations for specific cases of two-, three-, and four-component cases. Finally, Sec. IV gives a short summary and conclusion.

II. THEORY

A. Creating a moving BEC wave packet: Initial conditions

Figure 1 schematically shows the process of creating moving BEC wave packets via Bragg scattering wherein two sets of Bragg laser pulses create two moving daughter wave packets from an original condensate wave packet. Two laser

*Present address: Computer Sciences Corporation, 4090 S. Memorial Pkwy MS-918, Huntsville, AL 35815, USA.

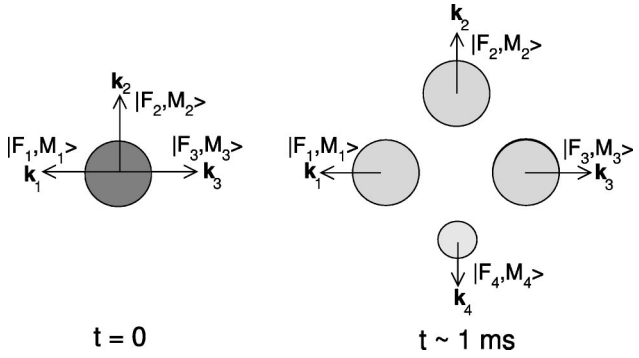

FIG. 1. Bragg scattering at time $t=0$ creates two moving daughter wave packets from the original parent condensate. In the center-of-mass frame in position space, shown in the figure, all three wave packets are moving with momenta of magnitude $\hbar|k|$ related to the photon recoil energy. The nonlinear interaction of the three initially created wave packets generates a fourth wave packet moving in the direction satisfying phase-matching criteria. At $t=1$ ms the four wave packets with spin states $|F_j,M_j\rangle$, $j=1,2,3,4$, have moved away from one another.

pulses of central frequency ω and $\omega+\delta$ and wave vector $\mathbf{k}_\omega$ and $\mathbf{k}_{\omega+\delta}$ incident on a gas of Bose-condensed atoms impart a well defined momentum "kick" to the atoms. We assume that the frequency ω is close to resonance with an atomic transition, and the detuning frequency δ is very small compared with ω. The frequency ω is chosen to be close to an allowed atomic transition (detuned by gigahertz), and δ for the pulse of central frequency $\omega+\delta$ is chosen to be in the kilohertz range. The angle between the propagation directions of the light pulses is θ ($\theta=180°$ corresponds to the counterpropagating pulses). We consider a parent condensate with atoms in a single internal spin state $|F_i,M_i\rangle$. A set of optical light pulses incident on the parent condensate with average momentum $\langle\mathbf{P}_0\rangle=\mathbf{0}$ can Bragg scatter atoms via Raman scattering from the initial wave packet, thereby creating a new daughter wave packet with momentum $\langle\mathbf{P}\rangle=\hbar(\mathbf{k}_\omega-\mathbf{k}_{\omega+\delta})$. This process is associated with absorption of one photon from the first pulse and stimulated emission of one photon into the second light pulse. This is a resonant transition and occurs only if conservation of energy and momentum are satisfied simultaneously. If the resulting velocity acquired by the atom is large compared to the speed of sound in the condensate, the dispersion relation is quadratic, and conservation of energy gives $\hbar\delta=P^2/2m+E_{F_f,M_f}-E_{F_i,M_i}$, where m is the atomic mass, and the subscripts f and i indicate the final and initial states, respectively. Conservation of momentum yields the relation $P=2\hbar k\sin(\theta/2)$, where $k=2\omega/c$; the atomic recoil momentum equals the difference between the central momenta of two pulses. It is often convenient to specify the velocity of the Bragg scattered atoms in units of the recoil velocity $v_R\equiv\hbar k/m$ (which equals 2.9 cm/s for ^{23}Na). The intensity and duration of the optical pulses determine the number of atoms that receive the recoil "kick" by undergoing the Raman process. The spin polarization and detuning of the lasers determine the final internal spin state $|F_f,M\rangle$. Two different sets of Bragg pulses are used to create two separate daughter wave packets. These, and what remains of the initial BEC, are the three nascent wave packets that participate in the FWM process.

The duration of the Bragg pulses is taken to be short (microsecond time scale) compared to the mean-field evolution of the BEC (typically hundreds of microseconds). As a result, it is easy to ensure conservation of energy and momentum in the Raman process that produces Bragg scattering. The whole momentum distribution of the initial BEC can therefore participate in the Bragg scattering process if the Bragg pulses are sufficiently short. We therefore use a "copy" approximation for the initial conditions of each slowly varying envelope created by Bragg scattering [3,8,9]. When the temporal widths of the Bragg pulses are sufficiently short so that the spectral widths of the Bragg pulses covers the whole range of velocities within the condensate, the copy approximation is an excellent approximation. The three nascent wave packets can be represented as $\Phi_r(\mathbf{x},0)=\sqrt{N_r(0)/N}\Psi_0(\mathbf{x},t=0)$, for $r=1,2,3$ at time $t=0$, $\Phi_4(\mathbf{x},0)=0$, where $\Psi_0(\mathbf{x},0)$ is the spatial component of the initial wave function, N is the total number of atoms, and $N_r(0)$ is the initial number of atoms in the rth component. Before the Bragg pulses are applied, all the atoms are in the same internal spin state. If the Bragg pulse sequence triggering the FWM process is associated with a change in the internal spin state of the atoms, the daughter wave packet has not only a different momentum from the parent, but also a different internal spin component. It is essential that the Raman detuning from the excited hyperfine state is smaller than the hyperfine splitting in order for Bragg pulses to change the internal spin state.

B. SVEA equations

Our zero-temperature theoretical model for FWM involves condensate dynamics described by the Gross-Pitaevskii equation (GPE) [10]. We start our analysis of different multispin component FWM processes by deriving a set of coupled GPEs for all the wave packets participating in the process. The Hamiltonian of the system in the second quantization can be written as

$$\hat{H}=\sum_\alpha\int\Psi_\alpha^\dagger(\mathbf{x},t)[T_\mathbf{x}+V(\mathbf{x},t)]\Psi_\alpha(\mathbf{x},t)d\mathbf{x}+\frac{1}{2}\sum_{\alpha,\beta,\gamma,\delta}\int\int\Psi_\alpha^\dagger(\mathbf{x},t)\Psi_\beta^\dagger(\mathbf{x}',t)U_{\alpha\beta,\gamma\delta}(\mathbf{x}-\mathbf{x}')\times\Psi_\gamma(\mathbf{x}',t)\Psi_\delta(\mathbf{x},t)d\mathbf{x}d\mathbf{x}', \quad (1)$$

where the subscripts $\alpha,\beta,\gamma,\delta$ denote different spin components. $T_\mathbf{x}=-(\hbar^2/2m)\nabla_\mathbf{x}^2$ is the kinetic energy operator, $V(\mathbf{x},t)$ is an external potential imposed on the atoms, and $U(\mathbf{x}-\mathbf{x}')$ is the interaction between particles, which for the dilute Bose gas is conventionally taken to be of contact form,

$$U_{\alpha\beta,\gamma\delta}(\mathbf{x}-\mathbf{x}')=\frac{4\pi\hbar^2a_{\alpha\beta,\gamma\delta}}{m}\delta(\mathbf{x}-\mathbf{x}'). \quad (2)$$

Here $a_{\alpha\beta,\gamma\delta}$ is the s-wave scattering length for the multispin collision process (see below) and m is the atomic mass. The

operators $\Psi_\alpha(\mathbf{x},t)$ satisfy equal time bosonic commutation relations

$$[\Psi_\alpha(\mathbf{x},t),\Psi_\beta(\mathbf{x}',t)]=[\Psi_\alpha^\dagger(\mathbf{x},t),\Psi_\beta^\dagger(\mathbf{x}',t)]=0, \tag{3}$$

$$[\Psi_\alpha(\mathbf{x},t),\Psi_\beta^\dagger(\mathbf{x}',t)]=\delta(\mathbf{x}-\mathbf{x}')\delta_{\alpha\beta}. \tag{4}$$

The Heisenberg equations of motion for all $\Psi_\alpha(\mathbf{x},t)$ fields can be obtained by taking the commutator with the Hamiltonian (1). We consider the case when the total wave function consists of four wave packets moving with different central momenta $\mathbf{P}_r=\hbar\mathbf{k}_r, r=1,\ldots,4$. Within a mean-field approximation we decompose the total wave function into separate wave packets, centered about momenta $\mathbf{P}_r$,

$$\Psi(\mathbf{x},t)=\sum_{r=1}^{4}\Phi_r(\mathbf{x},t)\exp(i\mathbf{k}_r\cdot\mathbf{x}-i\omega_r t)|\alpha_r, \tag{5}$$

where the rth wave packet with internal spin α_r and mean kinetic energy $\hbar\omega_r=\hbar^2k_r^2/2m$, $\Phi_r(\mathbf{x},t)$, is the slowly varying envelope (SVE) of packet r, $\hbar\mathbf{k_r}$ is the central momentum of packet r, and $|\alpha\rangle=|F_r,M_r\rangle$ labels the internal atomic spin state of the wave packet r.

Upon substituting the SVE expansion for Ψ in Eq. (5) back into the GPE, collecting terms, multiplying by the complex conjugate of the appropriate phase factors, and neglecting all terms that are not phase matched, thereby making the slowly varying envelope approximation [3], we obtain a set of coupled equations for the slowly varying envelopes $\Phi_r(\mathbf{r},t)$. The SVEA was necessary to restrict the momentum components only to those around the central momentum of each of the wave packets in the numerical calculation; otherwise, the momentum range would have been too large to treat numerically. Solving for the SVE allows efficient numerical simulations and helps in painting a clear picture of the process since it separates out explicitly the fast oscillating phase factors representing the central momentum $\hbar\mathbf{k}_r$. The SVEs $\Phi_r(\mathbf{x},t)$ vary in time and space on much longer scales than the phases. The multicomponent SVEA equations can be written as

$$\left[\frac{\partial}{\partial t}+(-\mathbf{v}_r)\cdot\boldsymbol{\nabla}+\frac{i}{\hbar}\left(-\frac{\hbar^2}{2m}\nabla^2+V_r(\mathbf{x},t)\right)\right]\Phi_r = \begin{cases} -\dfrac{i}{\hbar}NU_{rr,rr}|\Phi_r|^2\Phi_r \quad \text{(self-phase)}, \\ -\dfrac{i}{\hbar}N(1+\delta_{\alpha\beta})\displaystyle\sum_{s(s\neq r)}U_{rs,rs}|\Phi_s|^2\Phi_r \quad \text{(cross-phase)}, \\ -\dfrac{i}{\hbar}Nf_{\alpha\beta,\delta\gamma}\displaystyle\sum_{s,t,q(s\neq t\neq q\neq r)}U_{qr,st}\Phi_q^*\Phi_s\Phi_t \quad \text{(FWM source)}, \end{cases} \tag{6}$$

where $\alpha,\beta,\delta,\gamma$ are the respective spin components of wave packets q,r,s,t, and $f_{\alpha\beta,\delta\gamma}=2$ if all spin components are the same [11] (see also Sec. III A below), 1 if there are two or four distinct spin components, and $\sqrt{2}$ if there are three distinct spin components. We assume here that the scattering lengths that enter into the coupling constants in Eq. (2) are obtained from symmetrized scattering matrix elements, as described by Stoof *et al.* [12].

The interaction of the atoms with an external trapping field, which could be magnetic or optical, results in a harmonic oscillator potential $V_r(\mathbf{x},t)$ for each spin component. We allow for a time dependence of the potential in order to account for the turning off of the trapping field in the experiments we model.

We consider only the case of zero or extremely weak magnetic field, such that the magnetic Zeeman shift is very small compared to the recoil energy $\hbar k^2/2m$. In this case, assuming that the kinetic energy associated with the Bragg "kicks" is much larger than the chemical potential of the condensate, the momentum and energy conservation conditions have the form

$$\mathbf{k}_r+\mathbf{k}_q-\mathbf{k}_s-\mathbf{k}_t=\mathbf{0}, \tag{7}$$

$$k_r^2+k_q^2-k_s^2-k_t^2=0 \text{ (in the c.m. frame)}. \tag{8}$$

Each of the indices r,q,s,t may take values between 1 and 4. If there were a non-negligible Zeeman splitting in the energies of different spin components, then the energy conservation condition would need to be modified to take into account the energy released in the inelastic scattering process. In general, one would expect the prospects for FWM to be greatly diminshed if the packets have large relative velocities.

Given our assumption of zero magnetic field, Eqs. (7) and (8) are automatically satisfied in two cases: (a) $r=q=s=t$ (all indices are equal), or (b) $r=s\neq q=t$ (two pairs of equal indices). The corresponding terms describe what is called in nonlinear optics self- and cross-phase modulation terms respectively. The self- and cross-phase modulation terms do not involve particle exchange between different momentum components. They modify both the amplitude and phase of the wave packet through the mean-field interaction.

Particle exchange between different momentum wave packets occurs only when all four indices in the last term on the right-hand side of Eq. (6) are different. In this case, satisfying the conservation of momentum and energy is not automatic. FWM can be viewed as a process in which one particle is annihilated in each wave packet belonging to an initially populated pair of wave packets and simultaneously one particle is created in each of two wave packets of another pair, one of which is initially populated and the other is initially unpopulated. Hence, FWM removes one atom from each of the "pump" wave packets (without losing generality we may call them 1 and 3), and places one atom in the "probe" wave packet (we will call it wave packet 2) and one atom in the FWM output (wave packet 4). The bosonic stimulation of scattering mimics the stimulated emission of photons in an optical medium. The phase-matching conditions are particularly simple in the center-of-mass frame, defined by the conditions $k_1=k_3$, $k_2=k_4$, and $k_2=k_1$. This picture is a consequence of the nature of the nonlinear terms in the four SVEA equations.

For the case of multicomponent FWM, there is an additional degree of freedom that must be included. In this case there is a coupling between different internal spin compo-

nents, introducing new selection rules, namely,

$$F_1 = F_2 = F_3 = F_4 \text{ or } F_1 = F_2 \neq F_3 = F_4, \tag{9}$$

and additionally

$$M_1 + M_3 = M_2 + M_4. \tag{10}$$

The initial wave function is obtained from the numerical solution of the time-dependent GPE using an imaginary time propagation in the presence of the magnetic potential [3]. In the FWM experiments we model, after turning off the trapping potential, the BEC wave packet is allowed to freely evolve for a time T_E before the sets of Bragg pulses are applied to produce three initial wave packets with three different momenta. To model this, we propagate the initial wave packet (in real time) for a period of time T_E to provide the initial condition in Eq. (6). This free evolution causes a spatially varying phase to develop across the condensate as it expands in the absence of the trapping potential due to the mean-field interaction. Given the initial condition, the SVEA equations can be used to propagate the envelope function of each wave packet, using the same numerical method used to propagate the ordinary time-dependent GPE.

C. Nonlinear coupling constants and loss terms

The goal of this paper is to estimate the number of atoms in the created FWM wave packet in various realizations of the multi spin FWM experiments. To accomplish this goal we must first determine the nonlinear coupling constants $U_{qr,st}$ for ^{23}Na and ^{87}Rb in the $F=1$ and $F=2$ internal spin states that appear in the GPE. We performed the calculations of the strength of the nonlinear coupling constant $U_{rq,st}(k_{ts})$, which is determined by the following two-body scattering process:

$$|F_s, M_s\rangle + |F_t, M_t\rangle \rightarrow |F_q, M_q\rangle + |F_r, M_r\rangle, \tag{11}$$

at relative momentum $k_{st}=|\mathbf{k}_s-\mathbf{k}_t|$. The nonlinear coupling constant is defined by $U_{qr,st}(k_{st})/\hbar=(4\pi\hbar/m)(-T_{qr,st}/k)$, where $S=1+2iT$ is the unitary scattering matrix. For the *elastic collision* case, and for small values of relative momentum k_{st}, the coupling constant is

$$\frac{-T_{st,st}}{k_{st}} \approx a_{st} \equiv A_{st} - iB_{st}, \tag{12}$$

where a_{st} is the complex s-wave scatttering length [13]. The total elastic cross section is given by $\sigma_{\text{elastic}}=(1+\delta_{st})4\pi(A_{st}^2+B_{st}^2)$, and the total rate constant for inelastic collisions is $(K_2^{\text{total}})_{st}=\Sigma_{qr}\ (K_2)_{st\rightarrow qr}=(4h/m)B_{st}$. The elastic and inelastic collisional losses from the moving wave packets can be calculated using σ_{elastic} and K_2, as described in Ref. [4]. We calculate the various A_{st} and B_{st} values for ^{23}Na and ^{87}Rb collisions using standard coupled channel models of threshold scattering.

Insight into the nature of the four-wave mixing source terms can be obtained by using a scattering representation that is useful at low magnetic field, where the total angular momentum $\mathbf{F}_t=\mathbf{F}_1+\mathbf{F}_3+l=\mathbf{f}+l$ of the colliding pair of atoms is conserved in a collision. The T-matrix elements we need are for the case when two atoms collide in the internal spin levels (F_1,M_1), (F_3,M_3) and with relative angular momentum ℓ,m and end up in the levels (F_2,M_2), (F_4,M_4) with relative angular momentum ℓ',m'. We assume that the collision energy is low enough that only s waves contribute, so that $\ell=\ell'=0$, $m=m'=0$.

To obtain the relevant quantum numbers, first vector couple the $|F_1M_1\rangle$ and $|F_3M_3\rangle$ levels to obtain the resultant angular momentum $|F_1F_3f,M_1+M_3\rangle$ states, then vector couple the relative angular momentum $|\ell,m\rangle$ to get the total angular momentum states $|F_1F_3f,\ell,F_t,M_t=M_1+M_3+m\rangle$. The desired symmetrized T-matrix elements [12] are given in terms of the indices $\{F_1F_3f\ell F_t\}$ and are independent of the projection quantum numbers M_1,M_3,m,M_t.

The only significant collisions we need to consider are spin exchange collisions. These are possible only if the following selection rules are obeyed: $\ell=\ell'$, $m=m'$, $f=f'$, and $M_1+M_3=M_2+M_4$; for s waves $\ell=0$ and $f'=f=F_t$. The four-wave mixing source term is proportional to $a(st\rightarrow qr)=-T_{qr,st}/k_{st}$. Using the transformation of T-matrix elements to the total angular momentum basis [14–16], assuming $\ell=\ell'=0$, we obtain

$$\begin{aligned} &a(F_1M_1,F_3M_3 \\ &\quad\rightarrow F_2M_2,F_4M_4) \\ &\quad= \left(\frac{1+\delta_{F_1F_3}}{1+\delta_{F_1F_3}\delta_{M_1M_3}}\right)^{1/2}\left(\frac{1+\delta_{F_2F_4}}{1+\delta_{F_2F_4}\delta_{M_2M_4}}\right)^{1/2} \\ &\qquad\times\sum_f (F_2F_4f|M_2M_4,M_2+M_4) \\ &\qquad\times(F_1F_3f|M_1M_3,M_1+M_3)a^{(f)}(F_1F_3\rightarrow F_2F_4), \end{aligned} \tag{13}$$

where $(|)$ are Clebsch-Gordan coefficients. Clearly four-wave mixing is possible only if the collisions are energy degenerate: $F_2=F_1$ and $F_4=F_3$.

For one- and two-component four-wave mixing, where $M_1=M_3=M_2=M_4$ or $M_2=M_1$ and $M_4=M_3$, respectively, the product of Clebsch-Gordon coefficients is positive definite, and the sum will be of the same magnitude as the individual elements. On the other hand, for three- or four-component four-wave mixing, there will be terms with the product of the Clebsch-Gordon coefficients being positive and terms with the product being negative. In this case, the scattering length that controls the FWM source term in Eq. (6) will involve *differences* of scattering lengths of comparable magnitudes, and will tend to be much smaller than for the one- or two-component case. For example,

$$a(1-1,11\rightarrow 10,10)=\frac{\sqrt{2}}{3}[a^{(2)}(11\rightarrow 11)-a^{(0)}(11\rightarrow 11)], \tag{14}$$

$$\begin{aligned} &a(1-1,2-1\rightarrow 10,2-2) \\ &\quad=\frac{\sqrt{2}}{3}[a^{(3)}(12\rightarrow 12)-a^{(2)}(12\rightarrow 12)]. \end{aligned} \tag{15}$$

Inelastic energy-releasing exchange collisions are possible

TABLE I. Scattering lengths $a_{qr,st}$ in nanometers for the source nonlinear coupling constant $U_{13,24}$. The scattering lengths are given to the nearest 0.01 nm, although these numbers are not necessarily accurate to 0.01 nm. The small numbers, depending on differences of scattering lengths as in Eq. (15), are, in particular, subject to revision as improved threshold scattering models develop based on the most recent high quality experimental data.

Spin states	^{23}Na	^{87}Rb
1		
$\|1,-1\rangle_1+\|1,-1\rangle_3\rightarrow\|1,-1\rangle_2+\|1,-1\rangle_4$	2.89	5.63
2		
$\|1,-1\rangle_1+\|1,0\rangle_3\rightarrow\|1,-1\rangle_2+\|1,0\rangle_4$	2.89	5.63
$\|1,-1\rangle_1+\|2,0\rangle_3\rightarrow\|1,-1\rangle_2+\|2,0\rangle_4$	2.78	5.51
3		
$\|1,-1\rangle_1+\|1,1\rangle_3\rightarrow\|1,0\rangle_2+\|1,0\rangle_4$	0.14	−0.01
$\|2,1\rangle_1+\|2,-1\rangle_3\rightarrow\|2,0\rangle_2+\|2,0\rangle_4$	0.64	0.38
$\|2,+2\rangle_1+\|2,0\rangle_3\rightarrow\|2,1\rangle_2+\|2,1\rangle_4$	0.78	0.44
4		
$\|1,-1\rangle_1+\|2,-1\rangle_3\rightarrow\|1,0\rangle_2+\|2,-2\rangle_4$	0.59	0.09
$\|1,-1\rangle_1+\|2,0\rangle_3\rightarrow\|1,0\rangle_2+\|2,-1\rangle_4$	0.36	0.06
$\|2,1\rangle_1+\|2,0\rangle_3\rightarrow\|2,2\rangle_2+\|2,-1\rangle_4$	0.35	0.22

only for the cases $\{F_1F_3f\}=\{122\}$, $\{220\}$, and $\{222\}$ for ^{23}Na and ^{87}Rb. For ^{87}Rb, these loss collisions are anomously small [17–19] and we can set $B^{(f)}(F_1F_3)=0$.

Table I gives our calculated scattering lengths, based on coupled channel models of threshold collisions, which should be used in the $U_{qr,st}$ coupling constant that gives the source term for FWM in Eq. (6), i.e., $U_{qr,st}=4\pi a_{qr,st}\hbar^2/m$. We include several cases for ^{23}Na and ^{87}Rb involving one, two, three, and four spins. The three- and four-spin cases have significantly larger coupling constants for ^{23}Na than for ^{87}Rb, because scattering length differences in Eq. (15) tend to be much larger for the former case. The imaginary part of the complex scattering length for the source term is small compared to the real part, even for ^{23}Na collisions, and is not shown.

III. RESULT OF CALCULATIONS

A. One- and two-spin component FWM

In the numerical simulations we model a condensate comprised of magnetically trapped atoms without a discernible noncondensed fraction. We assume trap frequencies in the x, y, and z directions of 84, 59, and 42 Hz, as in Ref. [1]. After the magnetic trap is switched off, the condensate expands freely during a delay time T_E. Then the sequence of two sets of Bragg pulses creates two moving wave packets 2 and 3 in the laboratory frame, in addition to the initial stationary wave packet 1. One can change the momentum of the wave packets by changing the angle between the laser beams used for the Bragg outcoupling or by changing the laser frequencies. Our simulations neglect the detailed dynamics during the application of the Bragg pulses; instead, we assume that after the Bragg pulses are applied, each wave packet is a copy of the parent condensate wave function. This is a good approximation for Bragg pulses that are in the microsecond regime [9]. We shall consider the case where the initial three wave packets contain an equal number of atoms (except for the case corresponding to the original experiments [1] where the ratio is 3:7:3).

In the center-of-mass reference frame, all the wave packets (including the new FWM wave packet) move with the same velocity. In the one- and two-spin component cases the thresholds of the incoming and outgoing collision pairs coincide, i.e., $F_q+F_r=F_s+F_t$. Moreover, M_F is a good quantum number in the two-body collision requiring $M_q+M_r=M_s+M_t$ for all cases. The three initial wave packets can each be in an arbitrary internal spin state of the alkali-metal atom (for ^{23}Na or ^{87}Rb this is either $F=1$ or $F=2$). The FWM process preferentially populates the fourth wave packet in a spin state that satisfies the energy and angular momentum projection constraints.

Of all the possible combinations of spin states we can start with, we find two distinct classes of combinations: (1) at least two of the three initial wave packets are in the same spin state, or (2) all three wave packets are in different spin states. In both cases, the overlap of the coherently moving BEC packets 1 and 2 form a grating (either a density grating or a spin-density grating) that 3 diffracts off, producing a new wave packet 4. In the single spin case the number of atoms in the fourth wave packet is four times larger than in the two-spin case, $(N_4)_{1\ \mathrm{spin}}\sim 4(N_4)_{2\ \mathrm{spin}}$, even if the scattering lengths and initial numbers of atoms for these cases were exactly identical. The grating picture that explains the factor of 4 is as follows. For the one-spin state case, wave packets 1 and 2 form a grating and wave packet 3 can scatter off the grating to produce atoms that are in wave packet 4 (see Fig. 1), *and* wave packets 2 and 3 form a grating and wave packet 1 can scatter off the grating to produce atoms that are in wave packet 4. These two amplitudes *add up coherently* so the probability is four times the probability that would be obtained were there only one amplitude for producing the fourth wave. For the two-spin state case, if packet 1 (or 3) is the different spin state, it will scatter off the grating formed by 2 and 3 (1 and 2) and form the same spin state in a wave packet with momentum $\mathbf{k}_4$. The gratings are dynamical ones that change in time as atoms are removed from wave packets 1 and 3 and placed in wave packets 2 and 4.

The s-wave scattering lengths were used to form the nonlinear coupling constants $U_{qr,st}=4\pi a_{qr,st}\hbar^2/m$, and, in turn, these were used in our numerical simulations of FWM. Figure 2 shows the fraction of atoms in the newly generated wave packet, $f_4=N_4/N$, versus the total number of atoms in the parent condensate N for a number of different FWM processes. We assumed a free expansion time (i.e., the delay time) of $T_E=600$ μs, as in the experiment [1]. The strongest FWM conversion is obtained for $|1,-1\rangle_1+|2,0\rangle_3\rightarrow|1,-1\rangle_2+|2,0\rangle_4$ collisions of ^{87}Rb atoms, since this case has the largest s-wave scattering length in the source term. The saturation (and even decrease in the ^{87}Rb case) of the FWM fraction $f_4\equiv N_4/N$ with increasing N is clear from Fig. 2. The origin of this saturation is discussed in Ref. [3] and is due to the physical separation of the interacting wave packets, backconversion from the newly formed wave packet 4, and elastic and inelastic scattering loss processes.

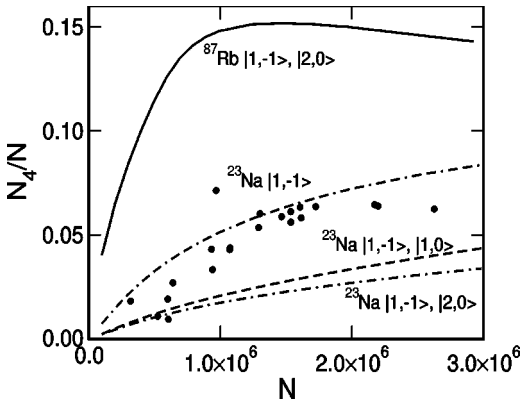

FIG. 2. Fractional FWM output versus total number of atoms N, $f_4=N_4/N$, in cases when one- or two-spin components are present. The simulations were carried out allowing the condensate to expand for 600 μs before applying the Bragg pulses, as in the experiment [1]. The solid circles are the experimental results obtained for ^{23}Na $|1,-1\rangle$. In the two-spin component simulations the ratio of atoms in the three initially populated wave packets are 1:1:1, whereas the one-spin component simulation used the experimental ratios of 7:3:7.

For reference, we included in Fig. 2 the original data from the experiment [1]. Comparison of the experimental results for ^{23}Na $|1,-1\rangle$ with the theoretical results show that at the highest values of N, the calculated number of atoms in the FWM wave packet is higher than in experiment. It is possible that stimulated elastic scattering loss may have to be taken into account at large N [4,20,21].

The scaling of the fraction of atom output into the FWM wave packet with $N_2(t_0)/N$ for $N=N_1(t_0)+N_2(t_0)+N_3(t_0)=N=1.5\times10^6$ is shown in Fig. 3 for the case of $|1,-1\rangle_1+|1,0\rangle_3\rightarrow|1,-1\rangle_2+|1,0\rangle_4$ collisions of ^{23}Na atoms. Note that on the left part of the figure $N_1(t_0)=N_3(t_0)>N_2(t_0)$, while on the right part of the figure $N_1(t_0)=N_2(t_0)>N_3(t_0)$. In Ref. [3], we discussed how the fraction of atoms in the FWM wave packet would scale with the initial number of atoms in the three nascent wave packets. There we showed how a simple argument predicts that the total FWM output fraction is given by

$$f_4=\frac{N_4(t_{col})}{N}\approx f_1f_2f_3\left(\frac{t_{col}}{t_{NL}}\right)^2, \tag{16}$$

where $f_i=N_i(t_0)/N$, t_{col} is the time for the wave packets to separate, and t_{NL} is the characteristic nonlinear time scale, $t_{NL}=\hbar/\mu$, where μ is the chemical potential. This is an upper bound on the FWM output, since the mutual interaction of the packets due to the self- and cross-phase modulation terms (the self- and cross-interaction energy terms) and the elastic and inelastic loss processes are not included in the estimate. The curve labeled $N_1N_2N_3/N^3$ in Fig. 3 is obtained using Eq. (16). It follows the calculated results rather well. Clearly, for cases where $N<1.5\times10^6$, one expects that the simple argument will provide as good an estimate.

The dependence of the fraction of atoms in the FWM wave packet on the velocity of the condensate wave packets is shown in Fig. 4 for the case of ^{23}Na $|1,-1\rangle_1+|1,0\rangle_3$

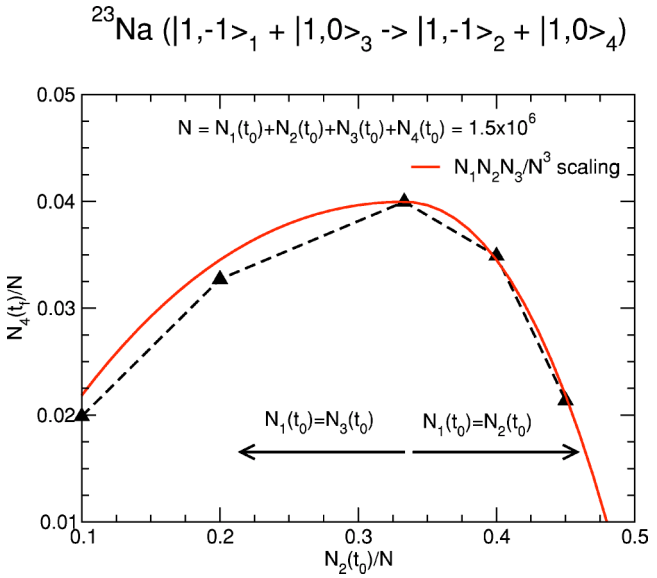

FIG. 3. Fractional FWM output versus $N_2(t_0)/N$. The solid curve is the result of using the simple model in Eq. (16) and the triangles are the result of calculations. The trap is the same as used in Fig. 2. The Bragg pulses are applied 300 μs after the trapping potential is turned off.

$\rightarrow|1,-1\rangle_2+|1,0\rangle_4$ condensate collisions where the free-expansion time T_E between trap off and the Bragg pulses is 300 μs. The velocities of the wave packets in the center-of-mass frame are indicated in Fig. 4 in units of the recoil velocity v_R (recall that the recoil velocity is defined as $v_R=\hbar k/m$ which equals 2.9 cm/s for ^{23}Na). The relative velocities of wave packets 1 and 3 or 2 and 4 are twice these velocities. As the relative velocity increases, the number of atoms in the FWM packet decreases, since the duration of the wave packet overlap essential to FWM decreases. For example, for the curve labeled $1.0v_R$ in Fig. 4 it takes about 500 μs for the centers of the moving wave packets to sepa-

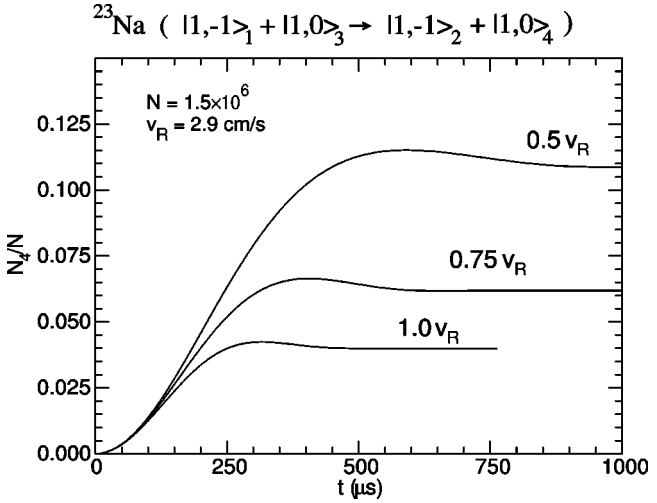

FIG. 4. $N_4(t)/N$ versus t for $N=1.5\times10^6$ atoms for various velocities $\hbar k/m$ of the wave packets. The trap is the same as used in Fig. 2. The Bragg pulses are applied 300 μs after the trapping potential is turned off.

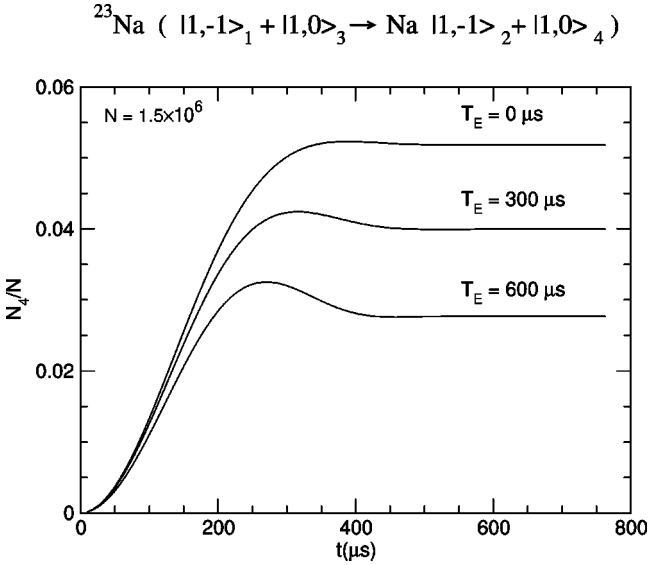

FIG. 5. $N_4(t)/N$ versus t for $N=1.5\times10^6$ atoms for various free-expansion times T_E. The trap frequencies are the same as used in Fig. 2.

rate by the mean Thomas-Fermi diameter of the initial condensate. The saturation of N_4/N is evident. For very slow relative velocities, N_4/N actually begins to decrease with time due to backconversion via FWM, as first described in Ref. [3].

The dependence of the fraction of atoms in the FWM wave packet on the free-expansion time T_E between turning off the harmonic potential and applying the Bragg pulses is shown in Fig. 5 for the case of ^{23}Na $|1,-1\rangle_1+|1,0\rangle_3\rightarrow|1,-1\rangle_2+|1,0\rangle_4$ condensate collisions when the wave packet velocity is $v_R=2.9$ cm/s. During the free expansion of the condensate, a spatially varying phase develops across the parent condensate, and this phase deleteriously affects the phase matching required for FWM. This has already been discussed in the single component studies that were published previously [3].

Figure 6 shows the total number of atoms in all the wave packets and the number of atoms in each of the wave packets during the FWM half collision versus time for the ^{87}Rb $|1,-1\rangle_1+|2,0\rangle_3\rightarrow|1,-1\rangle_2+|2,0\rangle_4$ case. A substantial loss of the condensate atoms due to elastic and inelastic scattering collisions occurs, but nevertheless the newly created FWM wave packet contains 120 000 atoms after full separation. This number of atoms can be easily detected. In fact, for all the cases shown in Fig. 2, the generated FWM signal is strong enough to be detected in real experiments when $N\geqslant1.0\times10^6$ atoms.

B. Three- and four-spin component FWM

FWM is possible with any combination of arbitrary internal spin states, provided M_F is conserved in the elastic two-body scattering process. FWM processes cannot be interpreted as Bragg diffraction off density gratings in three- or four-spin FWM. Instead, a "spin-polarization grating" scatters the atoms, as described above. For example, the four-mixing output (packet 4) in the process

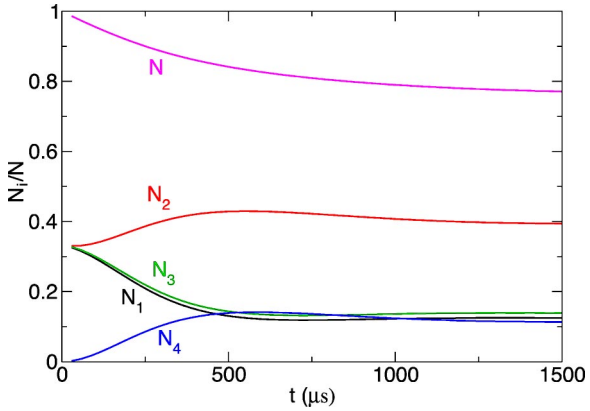

FIG. 6. $N(t)$, $N_1(t)$, $N_2(t)$, $N_3(t)$, and $N_4(t)$ versus t for ^{87}Rb$|1,-1\rangle_1+|2,0\rangle_3\rightarrow|1,-1\rangle_2+|2,0\rangle_4$ collisions with $N=1.0\times10^6$ atoms. The trap frequencies are the same as used in Fig. 2. The Bragg pulses are applied 600 μs after the trapping potential is turned off.

$$|1,-1\rangle_1+|1,1\rangle_3\rightarrow|1,0\rangle_2+|1,0\rangle_4 \tag{17}$$

can be thought of as a rotation of the "spin polarization" of wave packet 3 due to scattering off the spin-density grating formed by the overlap wave packets 1 and 2.

Figure 7 shows N_4/N versus N for ^{23}Na $|1,-1\rangle_1+|1,1\rangle_3\rightarrow|1,0\rangle_2+|1,0\rangle_4$ and for ^{23}Na $|1,-1\rangle_1+|2,-1\rangle_3\rightarrow|1,0\rangle_2+|1,-2\rangle_4$ condensate collisions. Figure 8 shows the time-dependent population fractions for the latter four-component case for $N=2.0\times10^6$ atoms. The s-wave scattering length in the source term for the former process is $a=0.14$ nm, whereas for the latter process $a=0.59$ nm. Taking an angle of 20° between the Bragg laser pulses ensures a relatively low velocity of $\hbar k/m=1$ cm/s for the moving packets. This allows the packets to remain overlapped long enough to generate an observable fourth wave.

IV. SUMMARY AND CONCLUSIONS

We have developed a general theory for describing four-wave mixing of matter-waves in arbitrary internal spin states within the context of a mean-field theory using the Gross-

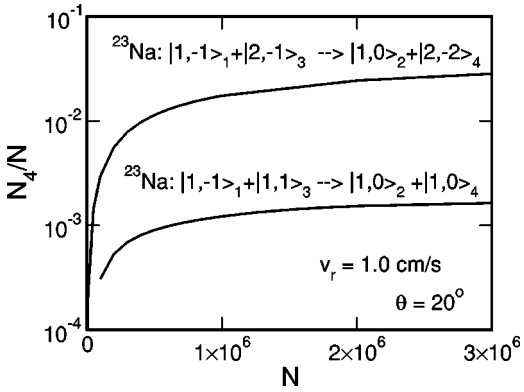

FIG. 7. Fractional FWM output versus total number atoms N calculated upon allowing the condensate to expand for 600 μs before applying the Bragg pulses for ^{23}Na $|1,-1\rangle_1+|1,1\rangle_3\rightarrow|1,0\rangle_2+|1,0\rangle_4$ and for ^{23}Na $|1,-1\rangle_1+|2,-1\rangle_3\rightarrow|1,0\rangle_2+|2,-2\rangle_4$. The initial ratio of atoms in the three populated wave packets are 1:1:1. The trap frequencies are the same as used in Fig. 2.

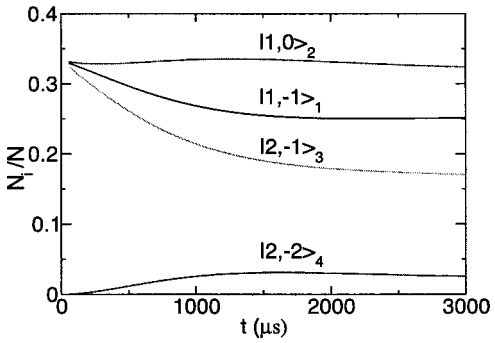

FIG. 8. $N_1(t)$, $N_2(t)$, $N_3(t)$, and $N_4(t)$ versus t for $N=2\times10^6$ atoms and ^{23}Na $|1,-1\rangle_1+|2,-1\rangle_3\rightarrow|1,0\rangle_2+|2,-2\rangle_4$. The trap frequencies are the same as used in Fig. 2. The Bragg pulses are applied 600 μs after the trapping potential is turned off.

Pitaevskii equation. The slowly varying envelope approximation is used to write separate equations for each of the condensate wave packets. The atom-atom interactions of the BEC atoms result in both the mean-field interaction terms, analogous to the self- and cross-phase modulation terms in nonlinear optics, and the FWM source terms in the GPE. The theory also incorporates elastic and inelastic scattering loss processes. These processes take atoms out of the condensate wave packets and therefore reduce the FWM. FWM with one- or two-spin states is analogous to Bragg diffraction of matter waves off a density grating formed by the moving BEC wave packets. The two-spin state FWM is generally smaller than the one-spin state case by a factor of about 4 due to the coherent addition of two amplitudes for scattering off the density gratings formed in the one-spin case, whereas only one scattering amplitude occurs for the two-spin state case. FWM with three- or four-spin states is generally a much weaker process; in the three- or four-spin state cases, the coherently moving BEC wave packets form a polarization grating (a spin-density grating) that rotates the spin projection of the diffracted wave.

Calculations of multicomponent FWM for ^{87}Rb and ^{23}Na condensate systems have been presented. In these calculations the three- and four-spin state FWM output signals are lower by roughly an order of magnitude than for one- and two-spin state FWM cases. The reduction is due to the much smaller source term for FWM in the three- and four-spin state cases, since the coupling strength involves differences of scattering lengths [see Eq. (15)] of comparable magnitudes.

ACKNOWLEDGMENTS

This work was supported in part by grants from the Office of Naval Research, the National Research Council, the U.S.-Israel Binational Science Foundation (Grant No. 2002147), and the Israel Science Foundation for a Center of Excellence Grant (Grant No. 212/01). M.T. acknowledges support from the Polish Ministry of Scientific Research and Information Technology under Grant No. PBZ-MIN-008/PO3/2003.

[1] L. Deng, E. W. Hagley, J. Wen, M. Trippenbach, Y. B. Band, P. S. Julienne, J. E. Simsarian, K. Helmerson, S. L. Rolston, and W. D. Phillips, Nature (London) **398**, 218 (1999).
[2] M. Trippenbach, Y. B. Band, and P. S. Julienne, Opt. Express **3**, 530 (1998).
[3] M. Trippenbach, Y. B. Band, and P. S. Julienne, Phys. Rev. A **62**, 023608 (2000).
[4] Y. B. Band, M. Trippenbach, J. P. Burke, and P. S. Julienne, Phys. Rev. Lett. **84**, 5462 (2000).
[5] J. H. Vogels, K. Xu, and W. Ketterle, Phys. Rev. Lett. **89**, 020401 (2002).
[6] E. Goldstein and P. Meystre, Phys. Rev. A **59**, 3896 (1999).
[7] Pierre Meystre, *Atom Optics* (Springer-Verlag, New York, 2001).
[8] M. Trippenbach *et al.*, J. Phys. B **33**, 47 (2000).
[9] P. B. Blakie and R. J. Ballagh, J. Phys. B **33**, 3961 (2000).
[10] F. Dalfovo *et al.*, Rev. Mod. Phys. **71**, 463 (1999).
[11] The factor of 2 was correctly used in the calculations reported in Ref. [3] , although inadvertently omitted from the source term on the right-hand side of the printed Eqs. (9) and (12)–(15) in that paper.
[12] H. T. C. Stoof, J. M. V. A. Koelman, and B. J. Verhaar, Phys. Rev. B **38**, 4688 (1988).
[13] P. S. Julienne, in *Scattering*, edited by R. Pike and P. Sabatier (Academic, New York, 2002), pp. 1043–1067.
[14] F. H. Mies, Phys. Rev. A **7**, 942 (1973).
[15] W. E. Baylis, J. Pascale, and F. Rossi, Phys. Rev. A **36**, 4212 (1987).
[16] K.-A. Suominen, E. Tiesinga, and P. S. Julienne, Phys. Rev. A **58**, 3983 (1998).
[17] P. S. Julienne, F. H. Mies, E. Tiesinga, and C. J. Williams, Phys. Rev. Lett. **78**, 1880 (1997).
[18] J. P. Burke, Jr., J. L. Bohn, B. D. Esry, and C. H. Greene, Phys. Rev. A **55**, R2511 (1997).
[19] S. J. J. M. F. Kokkelmans, H. M. J. M. Boesten, and B. J. Verhaar, Phys. Rev. A **55**, R1589 (1997).
[20] J. Steinhauer, R. Ozeri, N. Katz, and N. Davidson, Phys. Rev. Lett. **88**, 120407 (2002).
[21] R. Bach, M. Trippenbach, and K. Rzazewski, Phys. Rev. A **65**, 033811 (2002).